Local electric conductive property of Si nanowire models

Yuji Ikeda, Masato Senami, and Akitomo Tachibana

Citation: AIP Advances **2**, 042168 (2012); doi: 10.1063/1.4769887
View online: http://dx.doi.org/10.1063/1.4769887
View Table of Contents: http://scitation.aip.org/content/aip/journal/adva/2/4?ver=pdfcov
Published by the AIP Publishing

Local electric conductive property of Si nanowire models

Yuji Ikeda, Masato Senami, and Akitomo Tachibana[a]
Department of Micro Engineering, Kyoto University, Kyoto 606-8501, Japan

(Received 13 July 2012; accepted 20 November 2012; published online 28 November 2012)

Local electric conductive properties of Si nanowire models are investigated by using two local electric conductivity tensors, $\overleftrightarrow{\sigma}_{\rm ext}(\vec{r})$ and $\overleftrightarrow{\sigma}_{\rm int}(\vec{r})$, defined in Rigged QED. It is emphasized that $\overleftrightarrow{\sigma}_{\rm int}(\vec{r})$ is defined as the response of electric current to the actual electric field at a specific point and does not have corresponding macroscopic physical quantity. For the Si nanowire models, there are regions which show complicated response of electric current density to electric field, in particular, opposite and rotational ones. Local conductivities are considered to be available for the study of a negative differential resistance (NDR), which may be related to this opposite response. It is found that $\overleftrightarrow{\sigma}_{\rm int}(\vec{r})$ shows quite different pattern from $\overleftrightarrow{\sigma}_{\rm ext}(\vec{r})$, local electric conductivity defined for the external electric field. The effects of impurities are also studied by using the model including a Ge atom, in terms of the local response to electric field. It is found that the difference from the pristine model is found mainly around the Ge atom. [http://dx.doi.org/10.1063/1.4769887]

I. INTRODUCTION

Recently, semiconductor nanowires have gathered much attention since they have unique physical properties and can be applied in the fields of nano-electronics,[1–6] nano-optoelectronics,[7] and nano-photovoltics.[8] For instance, semiconductor nanowires are good candidates for next-generation materials of field effect transistor (FET) devices. Nanowire materials provide high electric conductance due to its ballistic conduction, and their structure is suitable for the suppression of the short channel effect by, for example, gate-all-around FET. Especially, Si nanowires are the leading candidate material for post-Moore devices[9–13] and have been studied intensively.

For electric conductive properties of nanosize materials, it is important to predict them by the first principles calculations before the fabrication in laboratories. In fact, many theoretical and computational studies have been performed for conductivity of nanomaterials. One of the most well-known approaches is non-equilibrium Green's function method.[14] By using this method, conductive properties of various nanodevices are analyzed.[15–18] These results show qualitatively sufficient consistency with experimental ones. However, we consider that this global and averaged conductivity for whole devices is not sufficient for understanding conductive properties of nanosize materials. For example, analysis by using global conductivity clarifies the effects of impurities only indirectly. Therefore, we have proposed the analysis by local quantities such as local dielectric constant tensor,[19–23] $\overleftrightarrow{\epsilon}(\vec{r})$, and local electric conductivity tensors,[24–27] $\overleftrightarrow{\sigma}_{\rm ext}(\vec{r})$ and $\overleftrightarrow{\sigma}_{\rm int}(\vec{r})$, which are defined in Rigged QED.[24,25] The use of local conductivity tensors enables us to discuss the effects of impurities or interface, and the position dependence of conductivity efficiently. In addition, local conductivity tensors help us to investigate the origins of some unusual electric phenomena, such as negative differential resistance (NDR) effect which been found for semiconductor nanowires[28–35] and molecular electronic devices.[36–38]

[a]E-mail address: akitomo@scl.kyoto-u.ac.jp

In our previous work,[27] we analyzed nanomaterials by only $\hat{\overleftrightarrow{\sigma}}_{\rm ext}(\vec{r})$ which represents the response to external electric field. In the present work, we show the validity of our analysis which uses both $\hat{\overleftrightarrow{\sigma}}_{\rm ext}(\vec{r})$ and $\hat{\overleftrightarrow{\sigma}}_{\rm int}(\vec{r})$, following our earlier works about the local quantity analyses.[19–27,39,40] It is especially noted that $\hat{\overleftrightarrow{\sigma}}_{\rm int}(\vec{r})$ is defined as the response of the electric current density to the internal electric field, and hence this does not have the corresponding macroscopic quantity. This quantity represents how the actual electric field at a specific position drives carriers such as electrons. This effect can never be analyzed by macroscopic conductivity. By using these two local electric conductivity tensors, we study electric conductive properties of Si nanowire models. In the present paper, we consider a pristine Si nanowire model and that which includes a Ge atom as an impurity.

In order to obtain the local electric conductivity tensors, the wave function of conductive electrons should be derived. However, most program codes for the calculations of electronic structures give us wave functions without net electric current. Hence, we must develop a calculation code to introduce electric current in a system. In our previous works, we developed a code which uses self-consistent field (SCF) procedure.[26,27] Effects of the conductive electrons on other ones were also considered in this code. In this work, we improve the method, based on a perturbation theory. By using this, we can calculate linear response to external electric field strictly.

This paper is organized as follows. In the next section, we define local electric current density and two conductivity tensors. In Sec. III, calculation method of our program code and computational models are summarized. In Sec. IV, we show results of our models in terms of our local electric conductivity tensors. Section V is devoted to the conclusion.

II. THEORY

A. Definition of the local properties

In this section, we show the definition of the local quantities for the response to the electric field. These quantities are introduced by Rigged QED.[24,25] We consider that a system (A) is embedded in an environmental background medium (M). The corresponding scalar potentials for A and M are given as the regional integrals of charge density,

$$\hat{A}_{0_{\rm A,M}}(\vec{r}) = \int_{\rm A,M} d^3\vec{s}\,\frac{\hat{\rho}(\vec{s})}{|\vec{r}-\vec{s}|}. \tag{1}$$

Here, $\hat{\rho}(\vec{r})$ is the electronic charge density defined as,

$$\hat{\rho}(\vec{r}) \equiv Z_e e \hat{\Psi}^\dagger(\vec{r})\hat{\Psi}(\vec{r}), \tag{2}$$

where e is the value of the elementary electric charge and $Z_e = -1$. The electric field $\hat{\tilde{E}}(\vec{r})$ is given as the sum of the electric displacement $\hat{\tilde{D}}(\vec{r})$ from M and the polarization $\hat{\tilde{P}}(\vec{r})$ of A. These quantities are defined with the scalar potentials of these regions,

$$\hat{\tilde{D}}(\vec{r}) = -\nabla \hat{A}_{0_{\rm M}}(\vec{r}), \tag{3}$$

$$\hat{\tilde{P}}(\vec{r}) = \frac{1}{4\pi}\nabla \hat{A}_{0_{\rm A}}(\vec{r}), \tag{4}$$

where the time variation of the vector component of gauge fields is dropped, since only steady states are treated in this work. As a result, the electric field is given as the following equation,

$$\hat{\tilde{E}}(\vec{r}) = \hat{\tilde{D}}(\vec{r}) - 4\pi\,\hat{\tilde{P}}(\vec{r}). \tag{5}$$

The electric displacement $\hat{\tilde{D}}(\vec{r})$ from M acts as the external electric field for A. Hence, the polarization of A is considered to be linear response to $\hat{\tilde{D}}(\vec{r})$,

$$\hat{\tilde{P}}(\vec{r}) = \hat{\overleftrightarrow{\alpha}}(\vec{r})\hat{\tilde{D}}(\vec{r}), \tag{6}$$

where $\overleftrightarrow{\alpha}(\vec{r})$ is the polarizability tensor. The dielectric constant tensor $\overleftrightarrow{\epsilon}(\vec{r})$ is given as,

$$\hat{\vec{D}}(\vec{r}) = \overleftrightarrow{\epsilon}(\vec{r})\hat{\vec{E}}(\vec{r}) = \frac{1}{1 - 4\pi\overleftrightarrow{\alpha}(\vec{r})}\hat{\vec{E}}(\vec{r}). \tag{7}$$

It is emphasized that $\overleftrightarrow{\alpha}(\vec{r})$ and $\overleftrightarrow{\epsilon}(\vec{r})$ are defined for every local point. There are several approaches which seems to be similar to our one. For example, Stone *et al.* have developed distributed polarizabilities.[41–43] This theory is often used for the purpose of inducing efficient intermolecular potential functions.[44,45] The advantage of our approach is its simple definitions of local quantities. They are quite similar to the definitions of corresponding macroscopic quantities.

From gauge covariant derivative, the local electric current density $\hat{\vec{j}}(\vec{r})$ can be given as,

$$\hat{\vec{j}}(\vec{r}) = \frac{Z_e e}{2m_e}[-i\hbar\hat{\Psi}^\dagger(\vec{r})\nabla\hat{\Psi}(\vec{r}) - \frac{Z_e e}{c}\hat{\Psi}^\dagger(\vec{r})\hat{\vec{A}}(\vec{r})\hat{\Psi}(\vec{r}) + h.c.]. \tag{8}$$

In our previous work,[26] we have shown that the effects of vector potential are negligible for small current density. Therefore, we ignore the vector potential in this work. Local electric conductivity tensors $\overleftrightarrow{\sigma}_{\text{ext}}(\vec{r})$ and $\overleftrightarrow{\sigma}_{\text{int}}(\vec{r})$ are defined as,[24,25]

$$\begin{aligned}\hat{\vec{j}}(\vec{r}) &= \overleftrightarrow{\sigma}_{\text{ext}}(\vec{r})\hat{\vec{D}}(\vec{r}) \\ &= \overleftrightarrow{\sigma}_{\text{ext}}(\vec{r})\overleftrightarrow{\epsilon}(\vec{r})\hat{\vec{E}}(\vec{r}) \\ &= \overleftrightarrow{\sigma}_{\text{int}}(\vec{r})\hat{\vec{E}}(\vec{r}),\end{aligned} \tag{9}$$

where $\hat{\vec{D}}(\vec{r})$ and $\hat{\vec{E}}(\vec{r})$ are external and internal electric field, respectively. As mentioned above, $\overleftrightarrow{\sigma}_{\text{int}}(\vec{r})$ represents how the actual electric field at each position drives electric carriers. This effect cannot be observed in macroscopic points of view. Some of computational works for the ballistic nanowire FET[46,47] have reported that the *I-V* characteristics of ballistic nanowires have a linear region, where the drain current I_D is proportional to the drain voltage V_D, and a saturation region, where I_D is independent of V_D. For the method in the present study, we assume the linear region.

In this study, local electric conductivity tensors are mainly investigated by their eigenvalues and eigenvectors. We also use the average of the eigenvalues as,

$$\sigma_{\text{Ave.}} = \frac{1}{3}(\sigma_1 + \sigma_2 + \sigma_3) = \frac{1}{3}\text{Tr}(\overleftrightarrow{\sigma}). \tag{10}$$

where σ_1, σ_2, and σ_3 are the first, the second, and the third eigenvalue, respectively. Each element in these tensors is a Hermitian operator and its expected value is real. These tensors, however, are not symmetric. For example, $\hat{\sigma}_{xy}(\vec{r})$ and $\hat{\sigma}_{yx}(\vec{r})$ may have different expected values. Hence, these tensors possibly have a pair of conjugate complex eigenvalues as,

$$\begin{aligned}\sigma_2 &= \beta + i\gamma, \\ \sigma_3 &= \beta - i\gamma, \ (\beta, \gamma \in \mathbb{R}).\end{aligned} \tag{11}$$

In such cases, the complex eigenvalues do not have the corresponding eigenvectors in real space. Instead, we can make two vectors from the complex eigenvectors as,

$$\vec{v}_+ = \frac{1}{\sqrt{2}}(\vec{v}_2 + \vec{v}_3), \tag{12}$$

$$\vec{v}_- = \frac{1}{\sqrt{2}i}(\vec{v}_2 - \vec{v}_3). \tag{13}$$

$\vec{v}_+$ and $\vec{v}_-$ are real vectors and respond to $\overleftrightarrow{\sigma}(\vec{r})$ as,

$$\overleftrightarrow{\sigma}\vec{v}_+ = \beta\vec{v}_+ - \gamma\vec{v}_-, \tag{14}$$

$$\overleftrightarrow{\sigma}\vec{v}_- = \beta\vec{v}_+ + \gamma\vec{v}_-. \tag{15}$$

We call this response of the local quantities as "rotational response". Rotational responses are also seen in our previous works.[21–23,27] The local property of rotational response is correctly described only in the analysis using matrix, since the complex eigenvalues originate in off-diagonal elements of the matrix.

III. CALCULATION METHODS

A. CPHF equations

In this study, the response to electric field is calculated by using Coupled Perturbed Hartree-Fock (CPHF) method.[48–50] CPHF method enables us to calculate linear response to external electric field strictly. In this subsection, the CPHF method used in this study is summarized.

First, the power series expansions of Hamiltonian $\boldsymbol{h}$ and density matrix $\boldsymbol{R}$ are given for the strength parameter of the perturbation λ as

$$\boldsymbol{h}(\lambda) = \boldsymbol{h}^{(0)} + \lambda \boldsymbol{h}^{(1)}, \tag{16}$$

$$\boldsymbol{R}(\lambda) = \boldsymbol{R}^{(0)} + \lambda \boldsymbol{R}^{(1)} + \cdots. \tag{17}$$

The corresponding first order Fock matrix $\boldsymbol{h}^{F(1)}$ can be defined as

$$\boldsymbol{h}^{F(1)} = \boldsymbol{h}^{(1)} + \boldsymbol{G}(\boldsymbol{R}^{(1)}), \tag{18}$$

where matrix $\boldsymbol{G}$ is the two-electron interaction defined as

$$G_{pq}(\boldsymbol{R}) = \sum_{r,s} R_{rs}\big([\psi_p\psi_q|\psi_r\psi_s] - [\psi_p\psi_s|\psi_r\psi_q]\big), \tag{19}$$

where the subscripts p, q, r, s are used for all molecular orbitals (MOs). Then, the first order CPHF equation is written as

$$(\epsilon_a - \epsilon_i)R^{(1)}_{ai} = -h^{F(1)}_{ai}, \tag{20}$$

where ϵ is the zeroth order orbital energy, and the subscripts a and i are used for the virtual and the occupied MOs, respectively. From Eqs. (18) and (19), it is clear that $\boldsymbol{h}^{F(1)}$ includes only the linear terms of $\boldsymbol{R}^{(1)}$ with respect to $\boldsymbol{R}$. Therefore, $\boldsymbol{R}^{(1)}$ can be obtained by solving simultaneous linear equations. In a similar way, the second order CPHF equation is represented as

$$(\epsilon_a - \epsilon_i)R^{(2)}_{ai} = -h^{F(2)}_{ai} + \sum_p \left(R^{(1)}_{ap}h^{F(1)}_{pi} - h^{F(1)}_{ap}R^{(1)}_{pi}\right). \tag{21}$$

B. Electronic structures with electric currents

Calculations of the electronic structures with electric currents are generally difficult. There are several approaches to deal with these structures. For example, Stuchebrukhov has developed the formalism of tunneling currents.[51–56] This theory is helpful to understand charge transfer systems in terms of interatomic currents. In this study, we calculate them by imposing some restriction to general CPHF method. In this subsection, this treatment is explained.

First, it is assumed that electron conduction is ballistic. Then, plane wave is considered as one of the simplest approximations for the conduction state. Therefore, conduction orbitals are considered to have the form,

$$\begin{aligned} |f^{(x)}(\vec{r})\rangle &= \exp(ik_x x), \\ |f^{(y)}(\vec{r})\rangle &= \exp(ik_y y), \\ |f^{(z)}(\vec{r})\rangle &= \exp(ik_z z), \end{aligned} \tag{22}$$

where $k_{x,\,y,\,z}$ are the parameters which correspond to the wave number vector. The extension of the direction perpendicular to momentum is restricted by the extension of virtual MOs of a system. In other words, $|f^{(x,y,z)}(\vec{r})\rangle$ are projected onto them as,

$$|\psi^{(i)}_{\mathrm{PW}}\rangle = C_{\mathrm{norm}} \sum_a |\psi_a\rangle\langle\psi_a|f^{(i)}(\vec{r})\rangle$$

$$= C_{\mathrm{norm}} \sum_a |\psi_a\rangle \sum_\mu C^*_{\mu a}\langle\phi_\mu|f^{(i)}(\vec{r})\rangle \qquad (i = x,\, y,\, z), \tag{23}$$

where the subscript μ is used for basis functions ϕ_μ, $C_{\mu a}$ is the expansion coefficients of the virtual MOs, and C_{norm} is the normalization coefficient. The spreads of the plane waves are suppressed by this procedure. In this study, $|\psi^{(i)}_{\mathrm{PW}}\rangle$ is regarded as the perturbation of the Highest Occupied MO (HOMO) $|\psi^{(1i)}_{\mathrm{HOMO}}\rangle$. This is given as,

$$|\psi^{(i)}_{\mathrm{HOMO}}\rangle = |\psi^{(0)}_{\mathrm{HOMO}}\rangle + d|\psi^{(1i)}_{\mathrm{HOMO}}\rangle + \cdots \tag{24}$$

$$= |\psi^{(0)}_{\mathrm{HOMO}}\rangle + d|\psi^{(i)}_{\mathrm{PW}}\rangle + \cdots \qquad (i = x,\, y,\, z), \tag{25}$$

where d is the perturbation mixing parameter related to the strength of the electric field, and $|\psi^{(0)}_{\mathrm{HOMO}}\rangle$ is an unperturbed HOMO. $|\psi^{(1i)}_{\mathrm{HOMO}}\rangle$ is fixed in corresponding CPHF equations, and the perturbation of the other occupied orbitals are determined as,

$$(\epsilon_a - \epsilon_j)R^{(1)}_{aj} = -h^{F(1)}_{aj}, \tag{26}$$

where the subscript j is used for occupied MOs except for the HOMO. The effect of the fixed wavefunction is included in $R^{(1)}_{ah}$ and $R^{(1)}_{ha}$, where the subscript h is used for the HOMO. In other words, the elements of $R^{(1)}_{ah}$ are not variables but constants in Eq. (26), which is different from Eq. (20).

The first order density matrix is dependent on the phase of $|f^{(x,y,z)}(\vec{r})\rangle$. Especially, if the phase changes by π, the sign of the first order density matrix $\boldsymbol{R}^{(1)}$ becomes opposite as,

$$\boldsymbol{R}^{(1)}(\theta + \pi) = -\boldsymbol{R}^{(1)}(\theta). \tag{27}$$

Therefore, the current caused by $\boldsymbol{R}^{(1)}$ also becomes opposite as,

$$\vec{j}^{(1)}(\vec{r};\theta + \pi) = -\vec{j}^{(1)}(\vec{r};\theta). \tag{28}$$

If the phase of $|f^{(x,y,z)}(\vec{r})\rangle$ can be taken arbitrarily and the average current caused by each phase is regarded as the real current, currents caused by the first order perturbation are equal to zero at all positions,

$$\vec{j}^{(1)}(\vec{r};\mathrm{Ave.}(\theta)) = 0. \tag{29}$$

On the other hand, the second order density matrix $\boldsymbol{R}^{(2)}$ does not change for the opposite phase. Hence in this study, currents caused by $\boldsymbol{R}^{(2)}$ for $\theta = 0$ is treated as the lowest order density matrix. The lowest order perturbation current is assumed to be derived from it.

$\vec{j}(\vec{r})$ by our method is strongly dependent on $k_{x,\,y,\,z}$ and d. In the present study, we choose the values of $k_{x,\,y,\,z}$ so that the difference between the projection of the plane waves on the virtual MOs and the original plane waves is relatively small. The value of d can be chosen so that $\vec{j}(\vec{r})$ is consistent with the macroscopic value obtained by experiments or other theoretical calculations such as the global current of non-equilibrium Green's function method. Accordingly, this value changes as the change of external field. However, the value of d does not change the distribution pattern of $\vec{j}(\vec{r})$. Hence we assume $d = 1$ and discuss the dependence on sites only qualitatively by using this method.

C. Calculation method for local properties

In this subsection, our calculation method for the local quantity tensors is given. First, CPHF calculations are done by using the perturbation Hamiltonians corresponding to the electric current

and external electric field,

$$\begin{aligned}\lambda_x \boldsymbol{h}^{(1x)} &= -\lambda_x D_0 Z_e e x,\\ \lambda_y \boldsymbol{h}^{(1y)} &= -\lambda_y D_0 Z_e e y,\\ \lambda_z \boldsymbol{h}^{(1z)} &= -\lambda_z D_0 Z_e e z,\end{aligned} \tag{30}$$

where x, y, z are the directions of the external electric field, D_0 is the unit electric field, and $\lambda_{x,\,y,\,z}$ are the strength parameters of the perturbation. The strength of the external electric field $D_{x,\,y,\,z}$ can be written as

$$D_j = \lambda_j D_0 \quad (j = x, y, z). \tag{31}$$

Then, density matrices $\boldsymbol{R}^{(2x,2y,2z)}$ are obtained. Local electric current density $\vec{j}(\vec{r})$ can be expanded as

$$\begin{aligned}j_i(\vec{r}, \lambda_x, \lambda_y, \lambda_z) = {} & j_i^{(0)}(\vec{r})\\ & + \lambda_x j_i^{(2x)}(\vec{r}) + \lambda_y j_i^{(2y)}(\vec{r}) + \lambda_z j_i^{(2z)}(\vec{r})\\ & + \cdots\\ & (i = x, y, z),\end{aligned} \tag{32}$$

where $j_i^{(2j)}(\vec{r})$ is caused by $\boldsymbol{R}^{(2)}$. By using this $\vec{j}(\vec{r})$, each element of $\overleftrightarrow{\sigma}(\vec{r})$ is calculated from Eq. (9). For instance, the value at $\vec{D}(\vec{r}) = 0$ is calculated as,

$$\begin{aligned}\sigma_{ij}(\vec{r}) &= \left.\frac{\partial j_i(\vec{r})}{\partial D_j}\right|_{D_j=0}\\ &= \left.\frac{\partial j_i(\vec{r})}{\partial \lambda_j}\frac{\partial \lambda_j}{\partial D_j}\right|_{D_j=0}\\ &= \frac{j_i^{(2j)}(\vec{r})}{D_0} \quad (i, j = x, y, z).\end{aligned} \tag{33}$$

Local polarizability tensor, $\overleftrightarrow{\alpha}(\vec{r})$, can be calculated in a similar way, and then $\overleftrightarrow{\epsilon}(\vec{r})$ is obtained from Eq. (7).

In order to analyze the characteristics of the local quantities in specific regions, spatial averages of the local quantities are calculated with the equations,

$$\langle\overleftrightarrow{\alpha}\rangle_V = \frac{1}{V}\int_V \overleftrightarrow{\alpha}(\vec{r})d\vec{r}, \tag{34}$$

$$\langle\overleftrightarrow{\varepsilon}\rangle_V = \frac{1}{1 - 4\pi\langle\overleftrightarrow{\alpha}\rangle_V}, \tag{35}$$

$$\langle\overleftrightarrow{\sigma}_{\text{ext}}\rangle_V = \frac{1}{V}\int_V \overleftrightarrow{\sigma}_{\text{ext}}(\vec{r})d\vec{r}, \tag{36}$$

$$\langle\overleftrightarrow{\sigma}_{\text{int}}\rangle_V = \langle\overleftrightarrow{\sigma}_{\text{ext}}\rangle_V\langle\overleftrightarrow{\epsilon}\rangle_V, \tag{37}$$

where V indicates the integral region. In the present paper, V is taken as a sphere around a specific atom. The scheme of the spherical average is shown in FIG. 1. In order to focus on the valence region of the atom and remove the effects of core electrons, we do not include the core of the sphere in the integral region. The radius of the core sphere, r_0, is taken to be 1 (bohr) for reference. In the present paper, the spherical average is analyzed as the function of the radius, r.

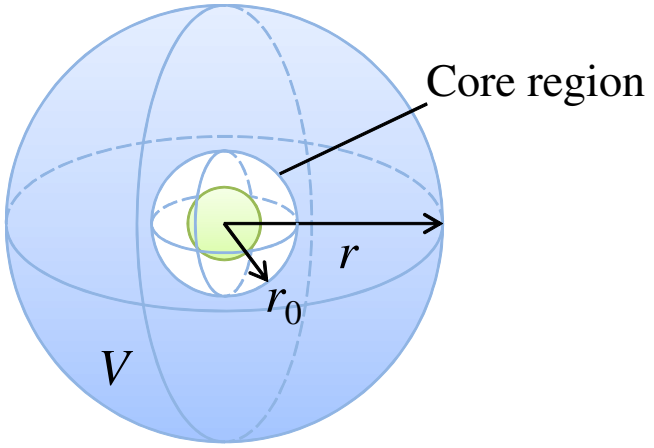

FIG. 1. Scheme of the spherical average around a specific atom.

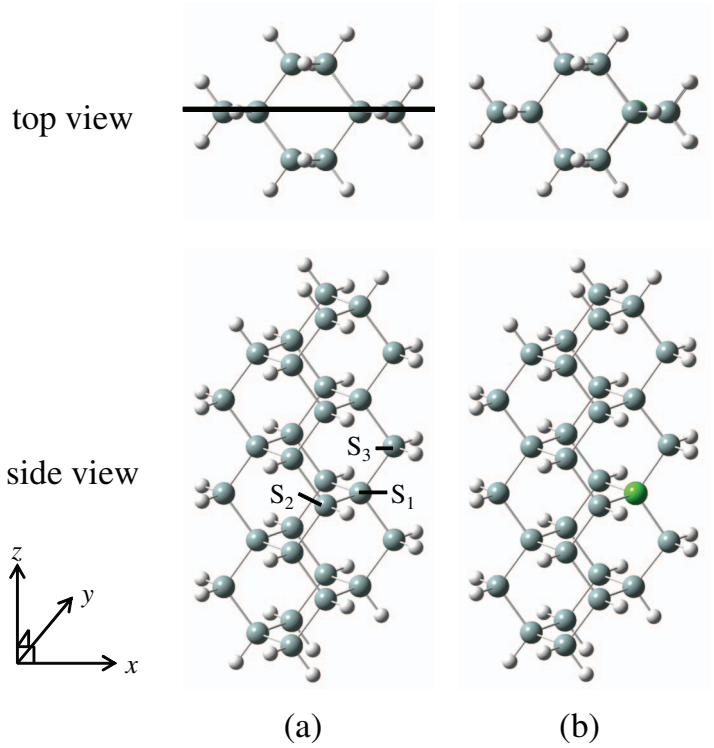

FIG. 2. Si nanowire models. Light-gray, green, and white spheres correspond to Si, Ge, and H atoms, respectively. (a) Pristine model and (b) Ge-substituted model. Thick line in panel (a) corresponds to *xz*-plane, where some results are shown on this plane in the following.

D. Computational models

In this subsection, computational models used in this study are shown. It has been reported that Si nanowires which have ⟨110⟩ growth direction have smaller electron and hole effective masses than those which have ⟨100⟩ or ⟨111⟩ growth direction.[57] Therefore in this work, we use Si nanowire models which have ⟨110⟩ growth direction.

In FIG. 2(a), our pristine Si nanowire model is shown. This model consists of eight layers. Each layer consists of three or four Si atoms. All dangling bonds are terminated with H atoms. Geometry is fully optimized. We also consider a model shown in FIG. 2(b). From the analysis of this model, we

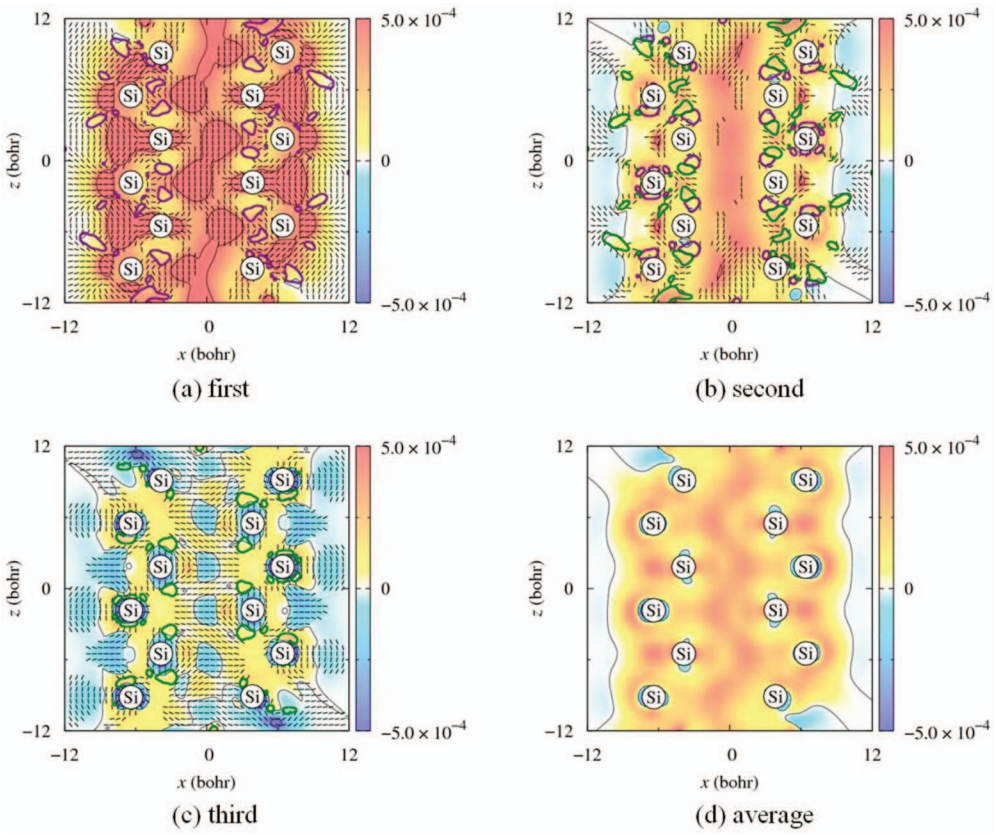

FIG. 3. Eigenvalues of $\overleftrightarrow{\sigma}_{\rm ext}(\vec{r})$ (a.u.) for the pristine model. Results are shown on the xz-plane. Eigenvalues are sorted in descending order of their real part. Panels (a), (b), and (c) show the results of the first, second, and third eigenvalues. Panel (d) shows the average of those three eigenvalues. The solid line segments show the directions of the eigenvectors. The eigenvalues in the purple (green) contours have positive (negative) complex values.

investigate the effects on the local electric conductivities caused by the change of the electronic and geometrical structures. For the model (b), the Si atom on site S_1 in FIG. 2(a), which makes bonds with four nearby Si atoms, is substituted by a Ge atom. All atoms are relaxed for the geometrical optimization calculation. The Model (b) is called the Ge-substituted model below in the present paper.

Electronic structures without perturbations (external electric field and electric current) are calculated by using the Hartree-Fock (HF) method, while those with perturbation Hamiltonians are calculated by CPHF method, as mentioned in this section. We choose the Dunning-Huzinaga double-zeta basis set with Effective Core Potential (ECP) by Hay and Wadt (LANL2DZ)[58–60] as basis set, and hence Si and Ge atoms in our models have ECP. Gaussian 09[61] is used for HF calculations, and CPHF calculations are done by using our original code. All local physical quantities are calculated at the vicinity of $\vec{D}(\vec{r}) = 0$. For the parameters $k_{x,\,y,\,z}$ in Eq. (22), they are taken as $k_{x,\,y,\,z} = 1.0\,(\text{bohr}^{-1})$ for reference, since the difference between the projection of the plane waves on virtual MOs and the original plane wave are relatively small for this value.

IV. RESULTS

A. Pristine model

In this subsection, we show the results for the pristine Si nanowire model. Local electric conductivity tensor for the external electric field, $\overleftrightarrow{\sigma}_{\rm ext}(\vec{r})$, on the xz-plane is shown in FIG. 3. We can find the regions which have negative eigenvalues, around Si atoms, the center axis of the nanowire,

and the exterior of it. In these regions, $\vec{D}(\vec{r})$ and $\vec{j}(\vec{r})$ show opposite directions. An important factor inducing negative eigenvalues is the large off-diagonal elements of $\overleftrightarrow{\sigma}_{\mathrm{ext}}(\vec{r})$. For example, this is seen at $\vec{r} = (8, 0, 0)$, which is at the surface of the nanowire. The value of $\overleftrightarrow{\sigma}_{\mathrm{ext}}(\vec{r})$ is given as,

$$\overleftrightarrow{\sigma}_{\mathrm{ext}}(8,0,0) = \begin{pmatrix} 0.44 & 0.00 & 2.07 \\ 0.00 & 1.07 & 0.00 \\ 1.93 & 0.00 & 3.93 \end{pmatrix} (\times 10^{-4}\,\mathrm{a.u.}). \tag{38}$$

It is found that the zx-element is larger than the xx-element. This means that when the external electric field is applied for the x-direction, the z-component of the current density is larger than the x-component. In addition, negative eigenvalues are seen in some unimportant regions, *e.g.*, around the center axis of the nanowire. In these regions, our basis set does not have enough degree of freedom for the accurate description, and hence we do not discuss those. Negative eigenvalues of $\overleftrightarrow{\sigma}_{\mathrm{ext}}(\vec{r})$ may be associated with NDR. It is considered that we can investigate the origin of NDR in more detail by using $\overleftrightarrow{\sigma}_{\mathrm{ext}}(\vec{r})$ than conventional global conductivity. In addition, if $\overleftrightarrow{\sigma}_{\mathrm{ext}}(\vec{r})$ is analyzed for various voltages, we can also study the dependence of NDR on voltage.

The regions which have complex eigenvalues are seen around Si atoms. As mentioned in Sec. II, $\vec{j}(\vec{r})$ responds to $\vec{D}(\vec{r})$ rotationally in these regions. For example, $\overleftrightarrow{\sigma}_{\mathrm{ext}}(\vec{r})$ at $\vec{r} = (4, 0, 1)$ is given as,

$$\overleftrightarrow{\sigma}_{\mathrm{ext}}(4,0,1) = \begin{pmatrix} 2.57 & 0.00 & 1.16 \\ 0.00 & 0.56 & 0.00 \\ -0.17 & 0.00 & 2.04 \end{pmatrix} (\times 10^{-4}\,\mathrm{a.u.}). \tag{39}$$

We can find that the signs of xz- and zx-elements are opposite, and the difference of xx- and zz-element are small. The rotational response is caused by these response properties. In our previous works, these responses are also seen in the results of $\overleftrightarrow{\sigma}_{\mathrm{ext}}(\vec{r})$ or $\overleftrightarrow{\epsilon}(\vec{r})$ of HfO_2, SiO_2, and so on.[21–23,27] Therefore, we consider that these characteristics are often seen in microscopic view.

Local electric conductivity tensor for the internal electric field, $\overleftrightarrow{\sigma}_{\mathrm{int}}(\vec{r})$, is shown in FIG. 4. Around Si-Si bonds, the third eigenvalues of $\overleftrightarrow{\sigma}_{\mathrm{int}}(\vec{r})$ has quite large negative eigenvalues, while those of $\overleftrightarrow{\sigma}_{\mathrm{ext}}(\vec{r})$ are positive there. It means that $\vec{j}(\vec{r})$ responds to $\vec{D}(\vec{r})$ in the same direction, while it responds to $\vec{E}(\vec{r})$ in the opposite direction. From the definition of $\overleftrightarrow{\sigma}_{\mathrm{int}}(\vec{r})$, which is shown in Eq. (9), it can be speculated that this difference is due to the effect of the local dielectric constant, $\overleftrightarrow{\epsilon}(\vec{r})$. Therefore it is helpful to analyze $\overleftrightarrow{\epsilon}(\vec{r})$ for the further understanding of the behavior of $\overleftrightarrow{\sigma}_{\mathrm{int}}(\vec{r})$ in these regions. The results of $\overleftrightarrow{\epsilon}(\vec{r})$ are shown in FIG. 5. As well as $\overleftrightarrow{\sigma}_{\mathrm{int}}(\vec{r})$, $\overleftrightarrow{\epsilon}(\vec{r})$ has negative eigenvalues around Si-Si bonds. In these regions, the polarization is significantly large and $\vec{E}(\vec{r})$ and $\vec{D}(\vec{r})$ show the opposite directions. If the eigenvalue of $\overleftrightarrow{\sigma}_{\mathrm{int}}(\vec{r})$ is negative, the change of $\vec{j}(\vec{r})$ at the position has the opposite direction to the change of $\vec{E}(\vec{r})$ for the direction of the corresponding eigenvector. Regions with negative $\overleftrightarrow{\sigma}_{\mathrm{int}}(\vec{r})$ impede the current.

Next, in order to discuss the site dependence of $\overleftrightarrow{\sigma}_{\mathrm{ext}}(\vec{r})$ and $\overleftrightarrow{\sigma}_{\mathrm{int}}(\vec{r})$, we show the spherical average of the local electric conductivity tensors. In FIG. 6, the spherical average of $\overleftrightarrow{\sigma}_{\mathrm{ext}}(\vec{r})$ around the three Si atoms on the sites $S_{1,2,3}$ in FIG. 2(a) are shown. We find that the third eigenvalues are negative or almost zero in the region of $1.0 < r < 2.0$ (bohr) for sites S_2 and S_3. This indicates that the electric current density $\vec{j}(\vec{r})$ may respond to the external electric field $\vec{D}(\vec{r})$ for the opposite direction or hardly respond to it for a specific direction. For the sites S_1 and S_3, we also find that all the eigenvalues are more scattered in the region of $1.0 < r < 2.0$ (bohr) than those in the region of $r > 2.0$ (bohr). This result means that the regions in the vicinities of the Si atoms on the sites S_1 and S_3 have relatively anisotropic properties. In order to analyze $\langle\overleftrightarrow{\sigma}_{\mathrm{ext}}\rangle_V$ in more detail, its eigenvalues and eigenvectors at $r = 1.25$, 2.00, and 4.00 (bohr) are summarized in TABLE I. We can find that the third eigenvectors for the sites S_2 and S_3 are almost correspond to the x-direction.

$\langle\overleftrightarrow{\sigma}_{\mathrm{int}}\rangle_V$ around the three Si atoms are shown in FIG. 7. It can easily be found that $\langle\overleftrightarrow{\sigma}_{\mathrm{int}}\rangle_V$ depends on r more heavily than $\langle\overleftrightarrow{\sigma}_{\mathrm{ext}}\rangle_V$. Due to this property, we can see the peak positions of the eigenvalues clearly. In order to discuss the difference between the sites in more detail, the results of

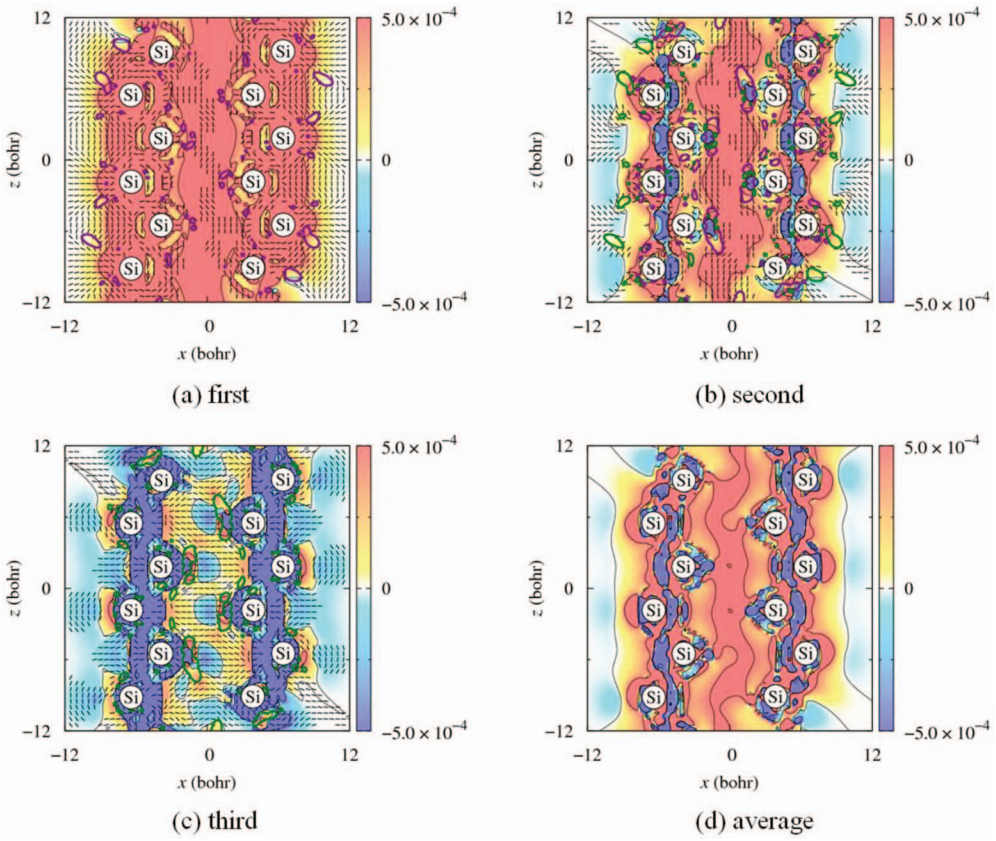

FIG. 4. Eigenvalues of $\overleftrightarrow{\sigma}_{\rm int}(\vec{r})$ (a.u.) for the pristine model. Results are shown on the same plane as FIG. 3 in the same manner. See the caption of FIG. 3 for the details.

$\langle\overleftrightarrow{\sigma}_{\rm int}\rangle_V$ at $r = 2.10$ (bohr) (covalent radius of a Si atom[62]) are summarized in TABLE II. It is found that the average of the eigenvalues for $\langle\overleftrightarrow{\sigma}_{\rm int}\rangle_V$ around the Si atom on the site S_3 is the largest of the all sites, followed by the sites S_1 and S_2. It is also clear that the standard deviation of the eigenvalues is the smallest for the site S_1. This is obviously because the Si atoms on the site S_1 have four Si-Si bonds, and therefore have more isotropic characteristics.

B. Comparison with the Ge-substituted model

In this subsection, we show the results for the Ge-substituted model and compare them with those for the pristine Si nanowire model. $\overleftrightarrow{\sigma}_{\rm ext}(\vec{r})$ of the Ge-substituted model is shown in Fig. 8. The difference from the results of the pristine model is mainly seen around the substituted atom. The eigenvalues around the Ge atom are smaller than those around the Si atom on site S_1 in the pristine model. This feature is also seen in the results of $\overleftrightarrow{\sigma}_{\rm int}(\vec{r})$, which are shown in Figs. 9.

In FIG. 10, we show the spherical average of $\overleftrightarrow{\sigma}_{\rm ext}(\vec{r})$ around the Ge atom in the Ge-substituted model. The eigenvalues and eigenvectors for three specific r are summarized in TABLE III. We can find that the difference between the eigenvalues of $\langle\overleftrightarrow{\sigma}_{\rm ext}\rangle_V$ is relatively moderate in the region of $r < 2.5$ (bohr), in comparison with the result of the Si atom on the site S_1 of the pristine model. In other words, $\langle\overleftrightarrow{\sigma}_{\rm ext}\rangle_V$ around the Ge atom is more isotropic than that of the Si atom on the site S_1 in the pristine model. We speculate that this result corresponds to the fact that the valence electrons of a Ge atom are bound to the nucleus more weakly than those of a Si atom: They can move more freely. For $r = 4.00$ (bohr), the values become similar to those of the Si atoms. This is because the effects nearby Si atoms are included in this result.

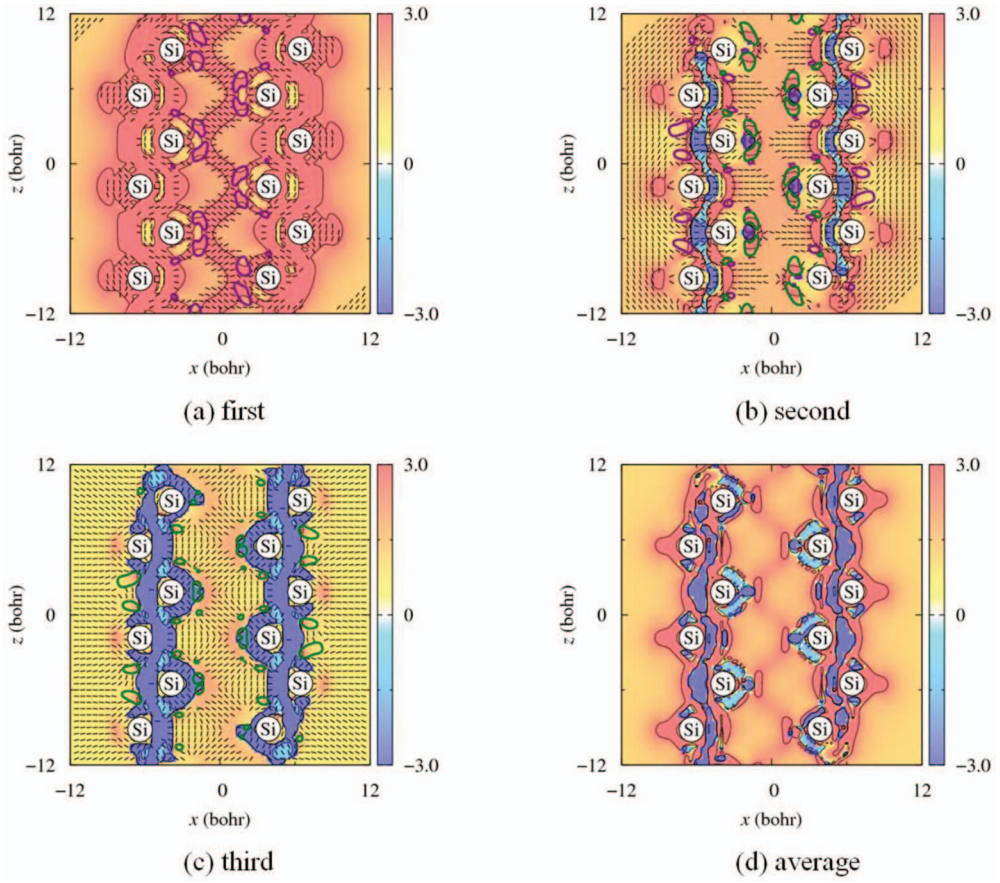

FIG. 5. Eigenvalues of $\overleftrightarrow{\epsilon}(\vec{r})$ for the pristine model. Results are shown on the same plane as FIG. 3 in the same manner. See the caption of FIG. 3 for the details.

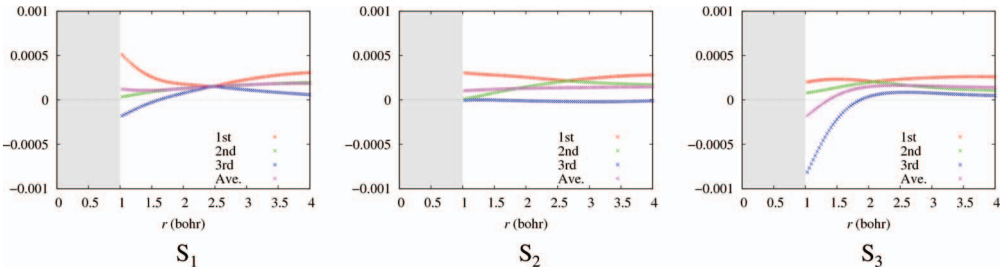

FIG. 6. Spherical average of $\overleftrightarrow{\sigma}_{\mathrm{ext}}(\vec{r})$ (a.u.) around three specific Si atoms on the sites $S_{1,2,3}$ shown in FIG. 2(a). The gray regions represent the core regions of the atoms.

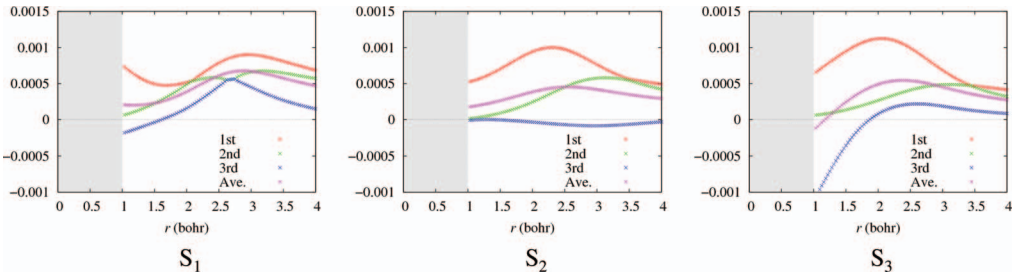

FIG. 7. Spherical average of $\overleftrightarrow{\sigma}_{\mathrm{int}}(\vec{r})$ (a.u.) around the Si atoms. Results are shown in the same manner as FIG. 6.

TABLE I. Eigenvalues ($\times 10^{-4}$ a.u.) and eigenvectors $\vec{v} = (v_x, v_y, v_z)^T$ of $\langle \overleftrightarrow{\sigma}_{\rm ext} \rangle_V$ at $r = 1.25$, 2.00, and 4.00 (bohr) for the Si atoms in the pristine model.

		S_1			S_2			S_3		
r		first	second	third	first	second	third	first	second	third
1.25	eigenvalue	3.672	0.614	−1.025	2.911	0.416	0.003	2.126	1.057	−4.978
	v_x	0.995	0.000	−0.038	−0.255	−0.151	0.961	0.000	0.013	1.000
	v_y	0.000	1.000	0.000	0.967	−0.066	0.244	1.000	0.000	0.000
	v_z	0.097	0.000	0.999	−0.018	0.986	0.131	0.000	1.000	0.009
2.00	eigenvalue	1.780	1.292	0.759	2.554	1.466	−0.109	2.112	1.975	0.369
	v_x	0.996	0.000	0.016	0.030	−0.012	1.000	0.000	0.023	1.000
	v_y	0.000	1.000	0.000	1.000	−0.009	−0.008	1.000	0.000	0.000
	v_z	0.085	0.000	1.000	0.008	1.000	0.008	0.000	1.000	0.002
4.00	eigenvalue	3.078	1.946	0.579	2.806	1.702	−0.111	2.599	1.066	0.487
	v_x	−0.001	0.000	0.999	0.001	0.012	1.000	0.005	0.000	1.000
	v_y	0.000	1.000	0.000	−0.004	1.000	0.021	0.000	1.000	0.000
	v_z	1.000	0.000	−0.045	1.000	0.006	−0.014	1.000	0.000	0.023

TABLE II. Eigenvalues, their averages, and the standard deviations (SDs) of $\langle \overleftrightarrow{\sigma}_{\rm int} \rangle_V$ ($\times 10^{-4}$ a.u.) at $r = 2.10$ (bohr).

	first	second	third	average	SD
S_1	5.49	5.37	2.10	4.32	1.57
S_2	9.71	2.82	−0.42	4.04	4.23
S_3	11.22	2.95	1.25	5.14	4.35

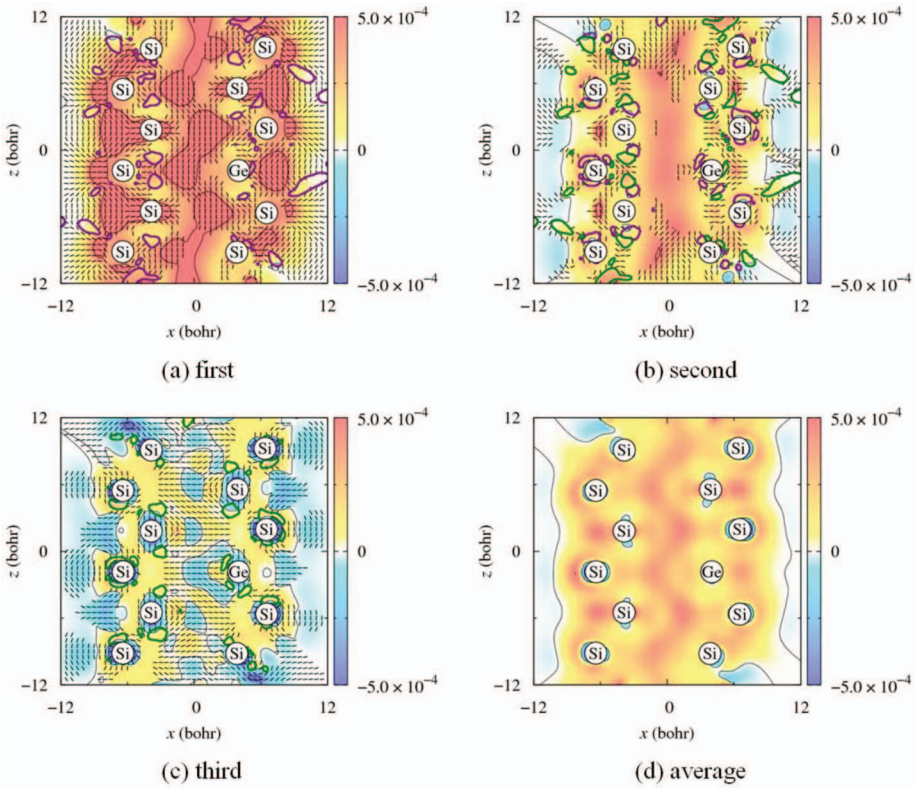

FIG. 8. Eigenvalues of $\overleftrightarrow{\sigma}_{\rm ext}(\vec{r})$ (a.u.) for the Ge-substituted model. Results are shown on the same plane as FIG. 3 in the same manner. See the caption of FIG. 3 for the details.

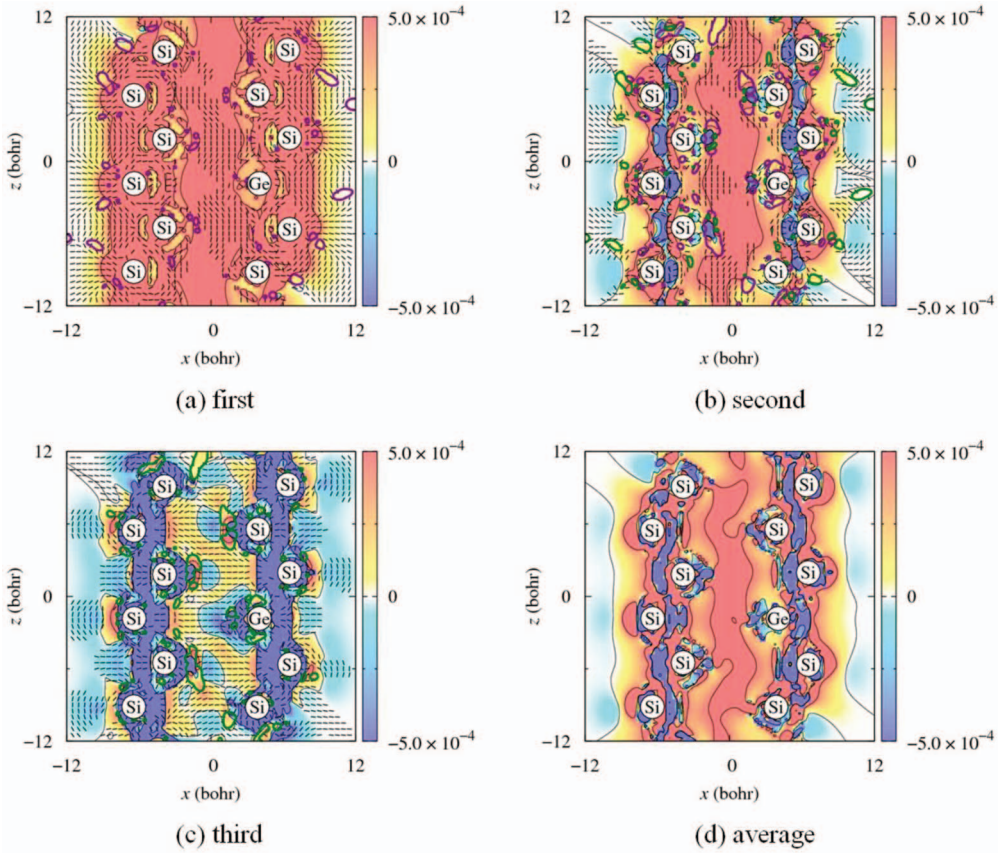

FIG. 9. Eigenvalues of $\overleftrightarrow{\sigma}_{\rm int}(\vec{r})$ (a.u.) for the Ge-substituted model. Results are shown on the same plane as FIG. 3 in the same manner. See the caption of FIG. 3 for the details.

Finally, we show the results of $\langle\overleftrightarrow{\sigma}_{\rm int}\rangle_V$ for the Ge-substituted model in FIG. 11. The results at $r = 2.27$ (bohr) (covalent radius of a Ge atom[62]) are also summarized in TABLE IV. The second and the third eigenvalues of $\langle\overleftrightarrow{\sigma}_{\rm int}\rangle_V$ around the covalent radius are close to each other for the Ge atom in the Ge-substituted model, while the first and second ones are close to each other for the Si atom at the site S_1 in the pristine model. This result represents a qualitative difference of the Si atom and the substituted Ge one. In addition, it can be found that both the first eigenvalue and the average of the eigenvalues at the covalent radius are larger than those the Si atom on the site S_1 for the pristine model. As mentioned above, this reflects the effect of the valence electrons of the Ge atom which can move more freely than those of the Si atom. It is also found that the standard deviation (SD) of the eigenvalues is larger than that of the Si atom on the site S_1 for the pristine model. Hence it can be said that $\langle\overleftrightarrow{\sigma}_{\rm int}\rangle_V$ around the Ge atom is more anisotropic than that of the Si atom on the site S_1 in the pristine model. This is the opposite result to that of $\langle\overleftrightarrow{\sigma}_{\rm ext}\rangle_V$ and clearly reflects the effect of anisotropic $\langle\overleftrightarrow{\epsilon}\rangle_V$.

V. CONCLUSION

In this work, we investigate the local response of Si nanowire models to the electric field. For this purpose, two local electric conductivity tensors, $\overleftrightarrow{\sigma}_{\rm ext}(\vec{r})$ and $\overleftrightarrow{\sigma}_{\rm int}(\vec{r})$, which are defined in Rigged QED, are used. We emphasize that $\overleftrightarrow{\sigma}_{\rm int}(\vec{r})$ can be defined as the electric current response to the internal electric field. $\overleftrightarrow{\sigma}_{\rm int}(\vec{r})$ does not have the corresponding macroscopic quantity. $\overleftrightarrow{\sigma}_{\rm int}(\vec{r})$ can represent how the actual electric field at a specific position drives carriers such as electrons. In order

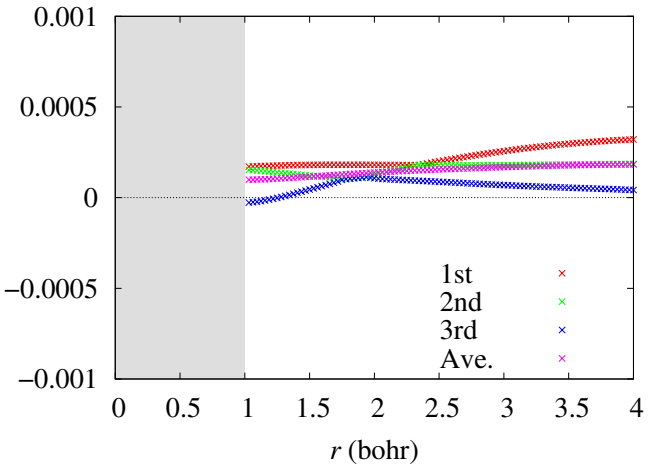

FIG. 10. Spherical average of $\overleftrightarrow{\sigma}_{\rm ext}(\vec{r})$ (a.u.) around the Ge atom in the Ge-substituted model. Results are shown in the same manner as FIG. 6.

TABLE III. Eigenvalues ($\times 10^{-4}$ a.u.) and eigenvectors $\vec{v} = (v_x, v_y, v_z)^T$ of $\langle \overleftrightarrow{\sigma}_{\rm ext} \rangle_V$ at $r = 1.25$, 2.00, and 4.00 (bohr) for the Ge atom in the Ge-substituted model.

r		Ge first	Ge second	Ge third
1.25	eigenvalue	1.769	1.389	−0.015
	v_x	0.000	0.991	−0.185
	v_y	1.000	0.000	0.000
	v_z	0.000	−0.136	0.983
2.00	eigenvalue	1.809	1.273	1.069
	v_x	0.000	0.164	0.868
	v_y	1.000	0.000	0.000
	v_z	0.000	0.987	0.497
4.00	eigenvalue	3.211	1.857	0.419
	v_x	0.001	0.000	1.000
	v_y	0.000	1.000	0.000
	v_z	1.000	0.000	−0.018

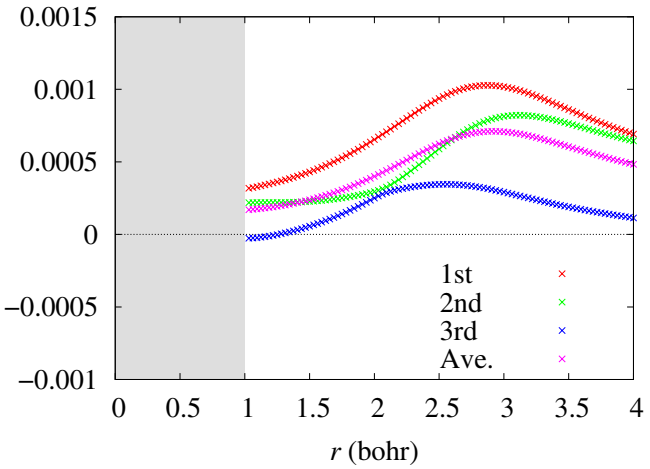

FIG. 11. Spherical average of $\overleftrightarrow{\sigma}_{\rm int}(\vec{r})$ (a.u.) around the Ge atom in the Ge-substituted model. Results are shown in the same manner as FIG. 6.

TABLE IV. Eigenvalues, their average, and their SD of $\langle \overleftrightarrow{\sigma}_{\rm int} \rangle_V$ ($\times 10^{-4}$ a.u.) at $r = 2.27$ (bohr) for the Ge atom in the Ge-substituted model.

first	second	third	average	SD
8.12	4.30	3.24	5.22	2.09

to investigate the effects of impurities for the local response to electric field, we consider both a pristine Si nanowire model and Ge-substituted one which include a Ge atom.

For the results of $\overleftrightarrow{\sigma}_{\rm ext}(\vec{r})$ and $\overleftrightarrow{\sigma}_{\rm int}(\vec{r})$ of the pristine Si nanowire model, there are the regions which show complicated response to the electric field, such as rotational one. For $\overleftrightarrow{\sigma}_{\rm ext}(\vec{r})$, there are the regions which show negative eigenvalues around the center axis of the nanowire and the exterior of it. On the other hand, for $\overleftrightarrow{\sigma}_{\rm int}(\vec{r})$, the regions around the Si-Si bonds also show negative eigenvalues. Spherical average of $\overleftrightarrow{\sigma}_{\rm ext}(\vec{r})$ around three specific atoms is also shown. We can see the site dependence of $\overleftrightarrow{\sigma}_{\rm ext}(\vec{r})$ clearly. From the analysis of $\langle \overleftrightarrow{\sigma}_{\rm int} \rangle_V$, it is clarified that the difference among the eigenvalues is the smallest for the site S_1. This is because the Si atoms on the site S_1 have four Si-Si bonds, and therefore have more isotropic characteristics.

$\overleftrightarrow{\sigma}_{\rm ext}(\vec{r})$ and $\overleftrightarrow{\sigma}_{\rm int}(\vec{r})$ of the Ge-substituted model show different features from the pristine model. The difference from the pristine model is seen mainly around the Ge atom, but this is relatively small. The spherical average of $\overleftrightarrow{\sigma}_{\rm ext}(\vec{r})$ and $\overleftrightarrow{\sigma}_{\rm int}(\vec{r})$ for the Ge-substituted model is also shown. It is found that $\langle \overleftrightarrow{\sigma}_{\rm ext} \rangle_V$ of the substituted Ge atom is more isotropic than that of the corresponding Si atom in the pristine model, while $\langle \overleftrightarrow{\sigma}_{\rm int} \rangle_V$ shows the opposite result. In this work, the conductive state is assumed to be represented as plane waves. To derive a more appropriate conductive state, we should improve the calculation code to realize conductive electronic states by more suitable boundary conditions, which is our future task.

ACKNOWLEDGMENTS

This work was partially supported by a Grant-in-Aid for Scientific Research from the Japan Society for the Promotion of Science (JSPS) (22550011). M. S. is supported by a Grant-in-Aid for Young Scientists (B) from JSPS (24760028) and Mizuho Foundation for the Promotion of Sciences. Y. I. is supported by the Sasakawa Scientific Research Grant from the Japan Science Society.

[1] Y. Cui and C. M. Lieber, Science **291**, 851 (2001).
[2] D. Wang, J. G. Lu, C. J. Otten, and W. E. Buhro, Appl. Phys. Lett. **83**, 5280 (2003).
[3] D. Wang, C. J. Otten, W. E. Buhro, and J. G. Lul, IEEE Trans. Nanotechnol. **3**, 328 (2004).
[4] D. Kang, J.-H. Ko, E. Bae, J. Hyun, W. Park, B.-K. Kim, J.-J. Kim, and C. Lee, J. Appl. Phys. **96**, 7574 (2004).
[5] H. Y. Cha, H. Wu, S. Chae, and M. G. Spencer, J. Appl. Phys. **100**, 024307 (2006).
[6] W. M. Zhou, F. Fang, Z. Y. Hou, L. J. Yan, and Y. F. Zhang, IEEE Electron Device Lett. **27**, 463 (2006).
[7] X. Duan, Y. Huang, R. Argarawal, and C. M. Lieber, Nature **421**, 241 (2003).
[8] B. Tian, X. Zheng, T. J. Kempa, Y. Fang, N. Yu, G. Yu, J. Huang, and C. M. Lieber, Nature **449**, 885 (2007).
[9] Y. Cui, L. J. Lauhon, M. S. Gudiksen, and J. Wang, Appl. Phys. Lett. **78**, 2214 (2001).
[10] Y. Wu, Y. Cui, L. Huynh, C. J. Barrelet, D. C. Bell, and C. M. Lieber, Nano Lett. **4**, 433 (2004).
[11] V. Schmidt, S. Senz, and U. Gösele, Nano Lett. **5**, 931 (2005).
[12] S. D. Suk, S.-Y. Lee, S.-M. Kim, E.-J. Yoon, M.-S. Kim, M. Li, C. W. Oh, K. H. Yeo, S. H. Kim, D.-S. Shin, K.-H. Lee, H. S. Park, J. N. Han, C. J. Park, J.-B. Park, D.-W. Kim, D. Park, and B.-I. Ryu, IEDM Tech. Dig. 2005, pp. 735.
[13] H. Lee, L.-E. Yu, S.-W. Ryu, J.-W. Han, K. Jeon, D.-Y. Jang, K.-H. Kim, J. Lee, J.-H. Kim, S. C. Jeon, G. S. Lee, J. S. Oh, Y. C. Park, W. H. Bae, H. M. Lee, J. M. Yang, J. J. Yoo, S. I. Kim, and Y.-K. Choi, Tech. Dig. VLSI Symp, 2006, pp. 58.
[14] S. Datta, in *Electronic Transport in Mesoscopic Systems*, edited by H. Ahmed, M. Pepper, and A. Broers (Cambridge University Press, Cambridge, England, 1995).
[15] J. Taylor, H. Guo, and J. Wang, Phys. Rev. B **63**, 121104 (2001).
[16] J. Taylor, H. Guo, and J. Wang, Phys. Rev. B **63**, 245407 (2001).
[17] P. S. Damle, A. W. Ghosh, and S. Datta, Phys. Rev. B **64**, 201403 (2001).
[18] M. Brandbyge, J.-L. Mozos, P. Ordejón, J. Taylor, and K. Stokbro, Phys. Rev. B **65**, 165401 (2002).
[19] K. Doi, Y. Mikazuki, S. Sugino, T. Doi, P. Szarek, M. Senami, K. Shiraishi, H. Iwai, N. Umezawa, T. Chikyo, K. Yamada, and A. Tachibana, Jpn. J. Appl. Phys. **47**, 205 (2008).

[20] P. Szarek, Ph.D. dissertation, Kyoto University, 2008.
[21] A. Fukushima, Y. Tsuchida, M. Senami, and A. Tachibana, Jpn. J. Appl. Phys. **49**, 111504 (2010).
[22] A. Fukushima, S. Sugino, Y. Tsuchida, M. Senami, and A. Tachibana, Jpn. J. Appl. Phys. **49**, 121504 (2010).
[23] M. Senami, Y. Tsuchida, A. Fukushima, Y. Ikeda, and A. Tachibana, Jpn. J. Appl. Phys. **51**, 031101 (2012).
[24] A. Tachibana, J. Mol. Model. **11**, 301 (2005).
[25] A. Tachibana, J. Mol. Struct.:THEOCHEM **943**, 138 (2010).
[26] M. Senami, Y. Ikeda, A. Fukushima, A. Tachibana, Jpn. J. Appl. Phys. **49**, 115002 (2010).
[27] M. Senami, Y. Ikeda, A. Tachibana, Jpn. J. Appl. Phys. **50**, 010103 (2011).
[28] J. Chen, M. A. Reed, A. M. Rawlett, and J. M. Tour, Science **286**, 1550 (1999).
[29] J. Chen, W. Wang, M. A. Reed, A. M. Rawlett, D. W. Price, and J. M. Tour, Appl. Phys. Lett. **77**, 1224 (2000).
[30] I. Amlani, A. M. Rawlett, L. A. Nagahara, and R. K. Tsui, Appl. Phys. Lett. **80**, 2761 (2002).
[31] I. Kratochvilova, M. Kocirik, A. Zambova, J. Mbindyo, T. E. Mallouk, and T. S. Mayer, J. Mater. Chem. **12**, 2927 (2002).
[32] K. Walzer, E. Marx, N. C. Greenham, R. J. Less, P. R. Raithby, and K. Stokbro, J. Am. Chem. Soc. **126**, 1229 (2004).
[33] A. M. Rawlett, T. J. Hopson, L. A. Nagahara, R. K. Tsui, G. K. Ramachandran, and Stuart M. Lindsay, Appl. Phys. Lett. **81**, 3043 (2002).
[34] A. M. Rawlett, T. J. Hopson, I. Amlani, R. Zhang, J. Tresek, L. A. Nagahara, R. K. Tsui, and H. Goronkin, Nanotechnology **14**, 377 (2003).
[35] J. D. Le, Y. He, T. R. Hoye, C. C. Mead, and R. A. Kiehl, Appl. Phys. Lett. **83**, 5518 (2003).
[36] C. Thelander, M. T. Björk, M. W. Larsson, A. E. Hansen, L. R. Wallenberg, L. Samuelson, Solid State Commun. **131**, 573 (2004).
[37] D. Lin, H. Wu, and Wei Pan, Adv. Mater. **19**, 3968 (2007).
[38] W.-H. Chu, H.-W. Chiang, C.-P. Liu, Y.-F. Lai, K.-Y. Hsu, and H.-C. Chung, Appl. Phys. Lett. **94**, 182101 (2009).
[39] M. Senami, J. Nishikawa, T. Hara, and A. Tachibana, J. Phys. Soc. Jpn. **79**, 084302 (2010).
[40] T. Hara, M. Senami, and A. Tachibana, Phys. Lett. A **376**, 1434 (2012).
[41] A. J. Stone, Mol. Phys. **56**, 1065 (1985).
[42] C. R. L. Sueur and A. J. Stone, Mol. Phys. **78**, 1267 (1993).
[43] C. R. L. Sueur and A. J. Stone, Mol. Phys. **83**, 293 (1994).
[44] A. J. Stone and C.-S. Tong, Chem. Phys. **137**, 121 (1989).
[45] G. J. Williams and A. J. Stone, J. Chem. Phys. **119**, 4620 (2003).
[46] K. Natori, J. Appl. Phys. **76**, 4879 (1994).
[47] K. Natori, IEEE Trans. Electron Devices **55**, 2877 (2008).
[48] R. M. Stevens, R. M. Pitzer, and W. N. Lipscomb, J. Chem. Phys. **38**, 550 (1960).
[49] J. Gerratt and I. M. Mills, J. Chem. Phys. **49**, 1719 (1968).
[50] D. B. Cook, *Handbook of Computational Quantum Chemistry* (Dover, New York, 2005), pp. 653–668.
[51] A. A. Stuchebrukhov, J. Chem. Phys. **104**, 8424 (1996).
[52] A. A. Stuchebrukhov, J. Chem. Phys. **105**, 10819 (1996).
[53] A. A. Stuchebrukhov, J. Chem. Phys. **107**, 6495 (1997).
[54] A. A. Stuchebrukhov, J. Chem. Phys. **108**, 8499 (1998).
[55] A. A. Stuchebrukhov, J. Chem. Phys. **108**, 8510 (1998).
[56] A. A. Stuchebrukhov, J. Chem. Phys. **118**, 7898 (2003).
[57] Y. Lee, T. Nagata, K. Kakushima, K. Shiraishi, and H. Iwai, in *2008 International Workshop on Dielectric Thin Films for Future Electron Devices*, Tokyo, Japan, 2008, pp. 83–84.
[58] P. J. Hay and W. R. Wadt, J. Chem. Phys. **82**, 270 (1985).
[59] W. R. Wadt and P. J. Hay, J. Chem. Phys. **82**, 284 (1985).
[60] P. J. Hay and W. R. Wadt, J. Chem. Phys. **82**, 299 (1985).
[61] M. J. Frisch, G. W. Trucks, H. B. Schlegel *et al.*, Gaussian 09, Revision B. 01. (Gaussian Inc., Wallingford CT, 2010).
[62] B. Cordero, V. Gómez, A. E. Platero-Prats, M. Revés, J. Echeverría, E. Cremades, F. Barragán, and S. Alvarez, Dalton Trans. **21**, 2832 (2008).